

# Commissioning and testing of pre-series triple GEM prototypes for CBM-MuCh in the mCBM experiment at the SIS18 facility of GSI

---

A. Kumar,<sup>a,b,1</sup> A. Agarwal,<sup>a,b</sup> S. Chatterjee,<sup>c</sup> S. Chattopadhyay,<sup>a,b</sup> A. K. Dubey,<sup>a,b</sup>  
C. Ghosh,<sup>a,b</sup> E. Nandy,<sup>a,b</sup> V. Negi,<sup>a</sup> S. K. Prasad,<sup>c</sup> J. Saini,<sup>a</sup> V. Singhal,<sup>a,b</sup> O. Singh,<sup>e</sup>  
G. Sikder,<sup>d</sup> J. de Cuveland,<sup>g</sup> I. Deppner,<sup>h</sup> D. Emschermann,<sup>f</sup> V. Friese,<sup>f</sup> J. Frühauf,<sup>f</sup>  
M. Gumiński,<sup>i</sup> N. Herrmann,<sup>h</sup> D. Hutter,<sup>g</sup> M. Kis,<sup>f</sup> J. Lehnert,<sup>f</sup> P.-A. Loizeau,<sup>f</sup>  
C.J. Schmidt,<sup>f</sup> C. Sturm,<sup>f</sup> F. Uhlig,<sup>f</sup> W. Zabołotny<sup>i</sup>

<sup>a</sup>Variable Energy Cyclotron Centre, Kolkata, INDIA

<sup>b</sup>Homi Bhabha National Institute, Mumbai, INDIA

<sup>c</sup>Bose Institute, Kolkata, INDIA

<sup>d</sup>University of Calcutta, Kolkata, INDIA

<sup>e</sup>Aligarh Muslim University, Aligarh, India

<sup>f</sup>GSI Helmholtz Center for Heavy-Ion Research GmbH (GSI), Darmstadt, Germany

<sup>g</sup>Frankfurt Institute of Advanced Studies (FIAS), Frankfurt am Main, Germany

<sup>h</sup>Physikalisches Institut, Ruprecht-Karls-Universität Heidelberg, Germany

<sup>i</sup>Institute of Electronic Systems, Warsaw University of Technology, Warsaw, Poland

E-mail: [akmaurya@vecc.gov.in](mailto:akmaurya@vecc.gov.in)

**ABSTRACT:** Large area triple GEM chambers will be employed in the first two stations of the MuCh system of the CBM experiment at the upcoming Facility for Antiproton and Ion Research FAIR in Darmstadt/Germany. The GEM detectors have been designed to take data at an unprecedented interaction rate (up to 10 MHz) in nucleus-nucleus collisions in CBM at FAIR. Real-size trapezoidal modules have been installed in the mCBM experiment and tested in nucleus-nucleus collisions at the SIS18 beamline of GSI as a part of the FAIR Phase-0 program. In this report, we discuss the design, installation, commissioning, and response of these GEM modules in detail. The response has been studied using the free-streaming readout electronics designed for the CBM-MuCh and CBM-STs detector system. In free-streaming data, the first attempt on an event building based on the timestamps of hits has been carried out, resulting in the observation of clear spatial correlations between the GEM modules in the mCBM setup for the first time. Accordingly, a time resolution of  $\sim 15$  ns have been obtained for the GEM detectors.

**KEYWORDS:** GEM, MuCh, mMuCh, FAIR, FAIR Phase-0, GSI, CBM, mCBM, data analysis, free-streaming

---

<sup>1</sup>Corresponding author.

---

## Contents

<b>1</b>	<b>Introduction</b>	<b>1</b>
<b>2</b>	<b>Design and fabrication of prototype GEM detectors</b>	<b>3</b>
<b>3</b>	<b>Experimental setup</b>	<b>4</b>
<b>4</b>	<b>Data analysis and first results</b>	<b>5</b>
<b>5</b>	<b>Summary</b>	<b>12</b>

---

## 1 Introduction

The Compressed Baryonic Matter (CBM) experiment [1] at the upcoming Facility for Antiproton and Ion Research (FAIR) in Darmstadt, Germany [2] is designed to investigate the properties of dense nuclear matter in nucleus-nucleus collision at an unprecedented interaction rate up to 10 MHz, which allows us to study extremely rare probes such as low mass vector mesons (LMVM), multi-strange hadrons and charmonia. The energy of the colliding beams will vary from 2-29 AGeV for proton and 2-14 AGeV for heavy-ion beams in the SIS100 ring of FAIR.

The Muon Chamber (MuCh) system [3] will be used to measure the dimuon signals originating from the heavy-ion collisions, which is one of the diagnostic probes to understand the physics of the fireball. MuCh consists of a series of segmented absorbers and detector stations sandwiched between them. A triplet of detector layers will be used in each station. A schematic diagram of the MuCh setup is shown in the left of Fig. 1, showing the detector layers and segmented absorbers. In the first two stations, owing to high particle flux, high rate detectors based on Gas Electron Multiplier (GEM) technology will be used [4–6]. GEM detectors have been chosen for particle detection in many experiments [7–11]. Likewise, in the CBM experiment, the role of the large area triple GEM detectors of MuCh is to carry out charged particle tracking for muon identification. The specifications of the GEM modules for the first two stations of MuCh are given in table 1. In any given layer, since the particle densities per unit area change when going radially outwards in the transverse direction from beam pipe, the pad-granularity of the GEM-MuCh module monotonically decreases from  $\sim 3.2$  mm pads in the inner region to about  $\sim 17$  mm on the periphery of the trapezoid for the modules of the first station, as can be visualized in Fig. 1 (right).

All detector systems of CBM will have to cope with very high interaction rates up to 10 MHz, in order to detect rare probes [12]. The maximum expected particle rate per unit area for the first station of MuCh is about  $400 \text{ kHz/cm}^2$  for minimum bias Au+Au collision at 10 AGeV beam energy. The signals from all the CBM detector subsystems will be read out using self-triggered electronics, enabling one to collect data at this high rate, whereby every signal above a set threshold is recorded along with the timestamp of these hits. Events are then reconstructed offline by grouping such hits

**Table 1.** Table for the specification of modules of the first two stations.

Station number	Number of layers	Total # of modules	Total # of readout channels	Total # of FEBs	Typical dimension of one module (cm) (active area)	Granularity (mm)
1	3	48	~107k	864	Inner ~7.5 Outer ~40.0 Length ~80.0	Min. ~3.2 Max. ~17
2	3	60	~109k	900	Inner ~7.9 Outer ~41.5 Length ~100.5	Min. ~4.5 Max. ~21.5

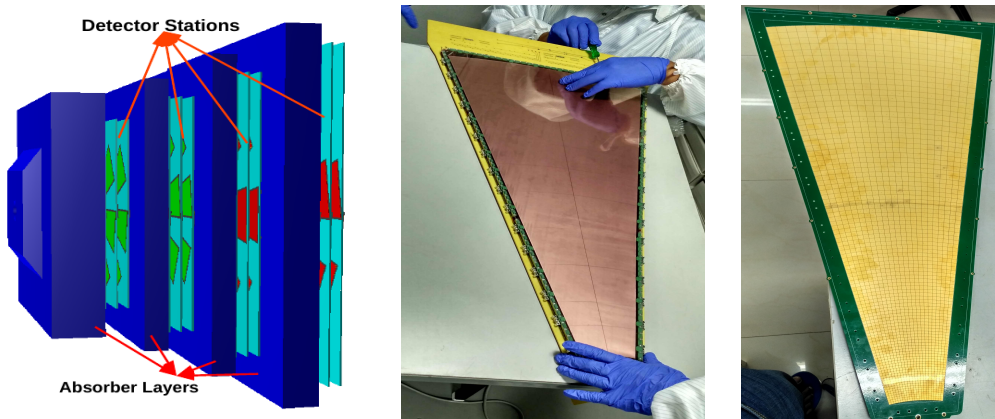


**Figure 1.** Left: Schematic of MuCh system in CBM. Middle: Chamber assembly. Right: Picture of the trapezoidal readout board for 1<sup>st</sup> station of MuCh.

28 in time. It, therefore, becomes essential to study an integrated response of the detectors through a  
 29 series of beam tests in which one studies in detail the performance of all the detector subsystems  
 30 of CBM prior to the actual experiment. In this regard, a precursor experiment consisting of all the  
 31 CBM detector subsystems has been setup at the SIS18 facility of GSI called mCBM [13] (“mini-  
 32 CBM”) as a part of the FAIR Phase 0 program. The mCBM experiment aims as a CBM full-system  
 33 test and enables tests of real-size modules of each detector subsystem under realistic experimental  
 34 conditions in high-rate nucleus-nucleus collisions. Major tasks are studying and optimizing the  
 35 DAQ and data transport to a computer farm, in particular, the timing-stability and data consistency  
 36 of the subsystem data streams, investigating issues related to the operation of detectors in a high-  
 37 rate environment, and developing and optimizing the software for online/offline data analysis. In  
 38 addition to this, the reconstruction of rare events like  $\Lambda$  Hyperon production in nucleus-nucleus  
 39 collisions at SIS18 energies will be performed.

40 In view of this, two real-size triple GEM detectors corresponding to the module sizes of  
 41 station-1 of MuCh were installed and commissioned in the mCBM experiment. Ar/CO<sub>2</sub> (70/30) gas  
 42 mixture has been the fill gas for the present tests. Tests with real-size detectors have been reported  
 43 in [6, 14]. However, the earlier tests were carried out with single-particle proton beams focused  
 44 at a specific location on the detector. At mCBM, the goal is to study the simultaneous response

45 from different regions of the detector and in conjunction with those from other subsystems when a  
 46 multitude of particles originating from nucleus+nucleus collisions pass through them. The first such  
 47 attempt was carried out at CERN-SPS [14], where the real-size modules used were of different gap-  
 48 configuration and were operated with different electronics compared to the present modules used  
 49 in mCBM. Moreover, the data at mCBM have been taken using the upgraded CBM DAQ [15] and  
 50 final readout ASIC, STS/MuCh-XYTER electronics [16, 17], which has been specifically designed  
 51 and developed for use by STS/MuCh subsystems in CBM.

52 Data were taken with Ar beams colliding on Au target of thickness 2.5 mm in November and  
 53 December 2019 beamtime. Preliminary results from the GEM-MuCh modules at mCBM have been  
 54 reported in [18]. In this paper, we report test results with the latest version of STS/MuCh-XYTER,  
 55 i.e., v2.1. The results discussed in this paper correspond mainly to a detector gain of about  $3.1 \times$   
 56  $10^3$ . The details of the GEM detector modules, their design, and fabrication are given in section 2.  
 57 The schematic of the experimental setup is described in section 3. The basic response of the  
 58 GEM chambers in terms of observing the spill structure using GEM modules, studying the time  
 59 synchronization of the detector hits, and the study of detector characteristics such as detector gain,  
 60 cluster size, etc., have been reported in section 4. The factors affecting the timing characteristics  
 61 have also been discussed in this section. We finally summarize in section 5.

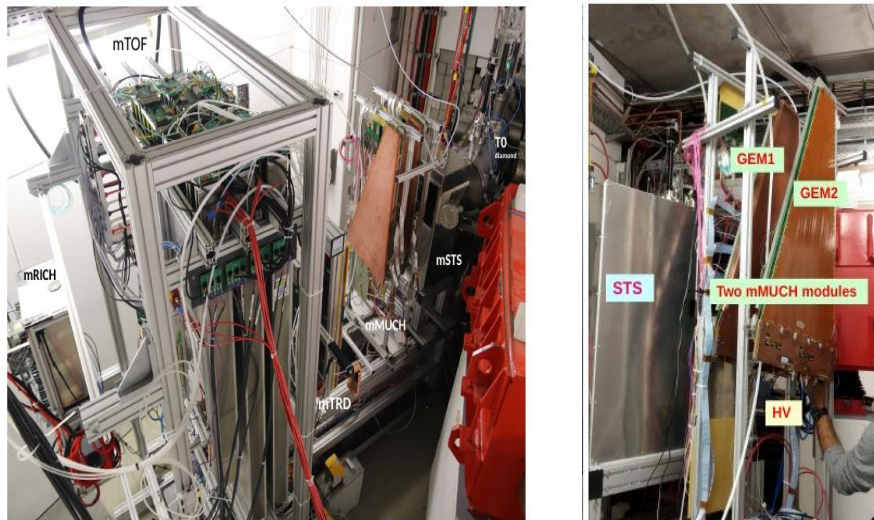


**Figure 2.** Left: Photograph of the experimental setup as of November 2019 showing the installed detector subsystems inside the mCBM cave at the SIS18 facility of GSI. Right: Closeup picture of two installed mMuCh modules.

## 62 2 Design and fabrication of prototype GEM detectors

63 Each of the two sector-shaped GEM chambers of mCBM consists of three GEM foils stacked in  
 64 a 3-2-2-2 gap configuration, where the number represents the gap between different layers in mm.  
 65 These modules have been designed and fabricated at VECC, Kolkata. Large size trapezoidal-  
 66 shaped, single-mask GEM foils were procured from CERN. These were stretched using the “NS-2”  
 67 technique [19], which does not use glue. The top surface of each foil is segmented into 24 divisions.

68 As part of essential Quality Assurance (QA) of the GEM foils, the foils were selected only when  
 69 they satisfied the criteria of no-short along with a low leakage current of  $<5$  nA at  $\Delta V_{GEM}$  of 550 V  
 70 for every segment. The measurement was done in air at an ambient temperature of about 23°C and  
 71 RH of around 45-50%. A novel optocoupler-based HV biasing scheme coupled to two resistive  
 72 chains was adopted for every module to power all the 24 foil segments. The optocoupler aims to  
 73 isolate any segment that may suddenly go bad in the course of operation, thus enabling the module  
 74 to function with the rest of the segments. Currently, “Dip-switches” are provided on the extended  
 75 portion of the drift PCB to isolate any segment whenever required physically. These, in the future,  
 76 would be coupled to micro-controller-based devices to control the on-off operation remotely. In  
 77 the mCBM campaign so far, no segment short has been observed in the GEM-MuCh modules. A  
 78 detailed discussion on optocoupler based design can be found in [20]. More details of the steps of  
 79 fabrication have been discussed in [6]. The active area of each of the trapezoidal detectors is about  
 80 1900 cm<sup>2</sup>, corresponding to 2231 pads. The entire detector module is read out using 18 front-end  
 81 boards (FEBs), each of which was connected to the pads in different regions on the detector plane.

### 82 3 Experimental setup

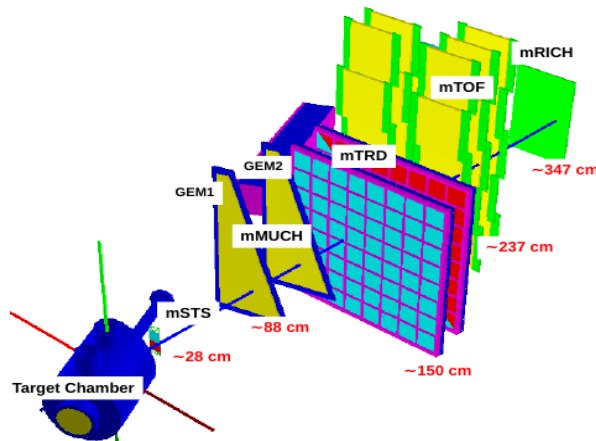


**Figure 3.** Schematic setup of mCBM experiment as of November 2019. Detectors are placed at approximately 25° from the beam axis. The diamond detector (T0) is placed inside the target chamber. mSTS - mini-Silicon Tracking System, mMuCh - mini-Muon Chamber System, mTRD - mini-Transition Radiation Detector, mTOF - mini-Time Of Flight, mRICH - mini-Ring Imaging Cherenkov.

83 A photograph of the two GEM modules as of November 2019, installed along with other  
 84 detector subsystems inside the mCBM cave located at the SIS18 facility of GSI, is shown in Fig. 2  
 85 (left). The subsystems were placed along the detector axis (25° line from beam direction) at different  
 86 distances from the target, the position of which is taken as the origin (0,0,0). All the detector centers  
 87 were (approximately) positioned at the height of 2 m from the ground and 25° from the beam axis.  
 88 Both mMuCh modules were mounted on an Al-plate of ~12 mm thickness. Each plate consisted of  
 89 ~6 mm Al-pipe winding inside the plate for carrying chilled water, thus providing the cooling of the  
 90 front-end boards (FEBs) [21]. A total of 18 FEB’s (front-end-boards) are needed to populate one  
 91 full chamber of station 1, with each FEB dissipating 2.5 W of heat. However, for the data reported

92 in this paper, the number of working FEBs was around 16 and 9 in GEM1 and GEM2, respectively.  
93 For the ease of installation, the dimensions of the Al-plates used in mCBM are slightly different  
94 from the actual design for the CBM experiment. The entire mMuCh system was then installed on  
95 the beam table, as shown in Fig. 2 (right). A schematic of the mCBM setup is shown in Fig. 3,  
96 typical distances of the detector subsystems are as shown. The diamond (T0) detector is placed  
97 inside the target chamber. The dimension of the T0 detector is approximately 20 mm x 20 mm and  
98 placed roughly at 20 cm upstream to the target. The mMuCh detectors were positioned with the  
99 readout side facing the target and oriented such that the long trapezoidal side was along the vertical  
100 axis, as shown in the figures. The detector axis intersected the modules at a distance of about 20 cm  
101 from the bottom edge of the trapezoid.

102 Signals from the readout pads of the mMuCh modules were sent via the readout connectors  
103 to the corresponding FEBs fixed on the Al-cooling plate, using 10 cm long flexible Kapton cables.  
104 These FEBs were then connected to the CBM DAQ system [15, 18]. In a free-streaming mode,  
105 signals from every electronic channel, whenever higher than a set threshold, are recorded along  
106 with their timestamps. The digitized signal from any electronic channel is referred to as Digi. The  
107 readout ASIC has 128 analog channels. Each channel uses a 5-bit Flash ADC, which was calibrated  
108 with a step size of 2.5 fC. Suitable thresholds were set to control the noise. Few channels in both  
109 modules were found to have exceptionally high noise and were masked before starting the data  
110 run. The ASIC does have a provision to set different thresholds to specific channels. However,  
111 implementing this in situ involves unplugging FEBs and re-calibrating the concerned channels,  
112 which is cumbersome. For studying the response from different areas of the detector at the same  
113 footing, a configuration with a common threshold for all channels is always preferred. Based on the  
114 observed noise behavior of the chambers, the thresholds of all the FEE boards were set to 6 fC, such  
115 that the noise rate stayed within the acceptable range of the usable bandwidth of the FEE boards.  
116 However, for a few boards in GEM2, a higher threshold had to be chosen.

## 117 **4 Data analysis and first results**

118 We report here the first results from data taken in November and December 2019 with  $^{40}\text{Ar}$  beam  
119 colliding on an Au-target of 2.5 mm thickness at an average intensity of  $5 \times 10^6$  per spill. A  
120 preliminary CBM data analysis chain based on the CbmRoot software framework [22] has been  
121 applied to the data. This involves raw data unpacking, including individual time-offset corrections  
122 for the detector subsystems (digis), a first event building by a timestamp cluster search and hit  
123 reconstruction for the detector subsystems. Using the Digi as well as the reconstructed hits,  
124 a dedicated analysis procedure was used to extract the mMuCh performance in dependence of  
125 various detector and analysis parameters.

126 The detector was operated at a summed GEM voltage of about 1072 V. The data were grouped  
127 in a time slice of size 10.24 ms. The typical distribution of signal counts from the GEM1 detector  
128 in time-bins (10 ms), taking the first hit time as a zero reference, is shown in the left panel of Fig. 4.  
129 The incident beam is in the form of spills, as displayed by the distribution of T0 counts. One notices  
130 that the raw counts in GEM1 (in green) do not display a proper spill structure. This is because  
131 of the large noise contribution, which is dominant in both on-spill as well as off-spill regions. An  
132 offline investigation of the off-spill data revealed that a few channels in some of the FEBs produced

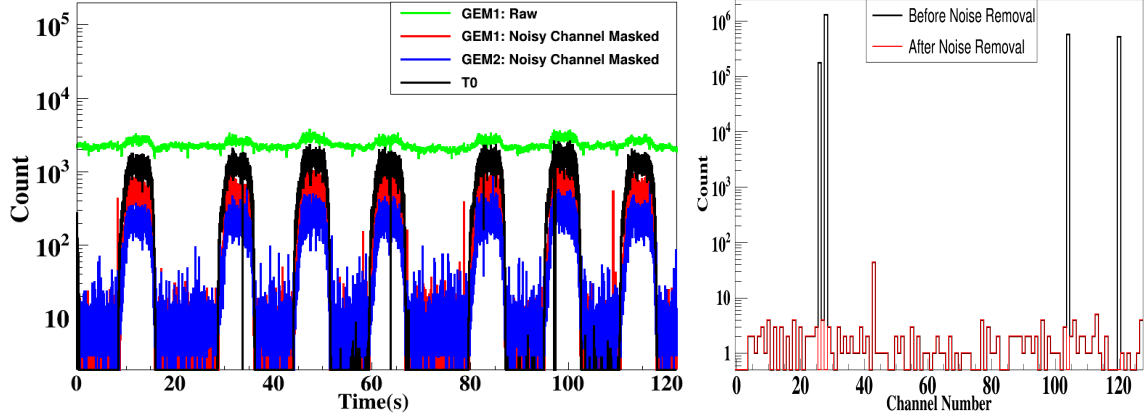


**Figure 4.** Left: Variation of Digi counts with time, spill structure, for GEM1-raw (green), GEM1/GEM2 - noise subtracted and T0. Right: Channel hit distribution for one of the FEB's in beam-off condition. Black corresponds to the raw channel count, and red is after masking noisy channels. Only a few channels are found to be noisy.

133 large noise, as can be seen from the channel-wise counts distribution for one FEB of GEM1 in  
 134 Fig. 4 (right). With the help of off-spill data, such noisy channels were identified in all ASIC's  
 135 and were accordingly masked for further analysis. The signal-counts distribution, after removal of  
 136 noisy channels for GEM1 (red), GEM2 (blue) reveal the spill structure (Fig. 4 (left)). They are now  
 137 observed to be well correlated with those of T0, as expected. The residual count still remaining in  
 138 the off-spill region is indicative of the noise rate and is observed to vary from one FEB-to-FEB.  
 139 Also, a higher noise level for GEM2 was observed as compared to GEM1. However, these are of  
 140 much lower counts than the counts in the on-spill region.

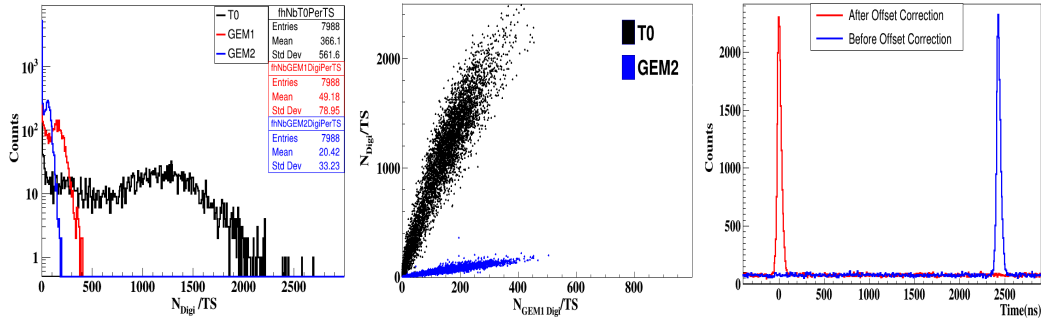


**Figure 5.** Left: Distribution of the number of digis per time-slice (Digi/TS) for GEM1 (red), GEM2 (blue) and T0 (black). Middle: Variation of the number of T0 Digi/TS with GEM1 Digi/TS (red) and the number of GEM2 Digi/TS with GEM1 Digi (blue). Right: Time difference distribution between one FEB of GEM1 with T0 before (blue) and after (red) offset correction (see text).

141 The extracted spill length of the beam is about 7 s, with off-spill lengths of approximately 7 s  
 142 and 12 s, (parallel user operation) as can be noticed in Fig. 4, left side. As has been mentioned, the  
 143 data were collected in 10 ms Time-Slice (TS) intervals. The distribution of the number of digis per  
 144 TS for the two GEM modules and T0 is shown in Fig. 5 (left). This includes counts in the off-spill  
 145 region as well, which being relatively much lower, show up in the form of a peak at values around  
 146 10-30 Digi/TS for both the GEM modules, while the peaks on the higher side of the spectra are

147 due to signals from on-spill. A difference between these two peaks provides the average number  
 148 of digis/TS for any detector, corresponding to the particular operating conditions at which the data  
 149 was taken. The on-spill peak for GEM2 is lower than that of GEM1 because of its lower acceptance  
 150 owing to the smaller number of working FEBs. The correlation in terms of the number of digis per  
 151 TS between the three subsystems is shown in the middle panel of the same figure.

152 Each collision is a point in time. Hence the digis from different detector subsystems should be  
 153 correlated in time. This is revealed from the time difference spectra shown in Fig. 5 (right, blue)  
 154 where, within every time slice interval, the time difference distribution between the digis from a  
 155 FEB of GEM1 and T0 has been plotted. This represents a typical time-correlation spectra. The  
 156 mean position of this distribution (around 2500 ns) represents the offset for the particular FEB, and  
 157 this varies from one FEB to another. Synchronizing all the hits from different FEBs becomes thus  
 158 essential for a proper data analysis. In this direction, time offset for all the FEBs corrections need  
 159 to be properly determined. The offset-value is subtracted from timestamps of each Digi for the  
 160 corresponding FEB, such that the resulting time-corrected distribution now peaks at zero, as per  
 161 construction (represented by the red curve in Fig. 5 (right)). Such offset corrections were applied  
 162 for all subsystems separately.

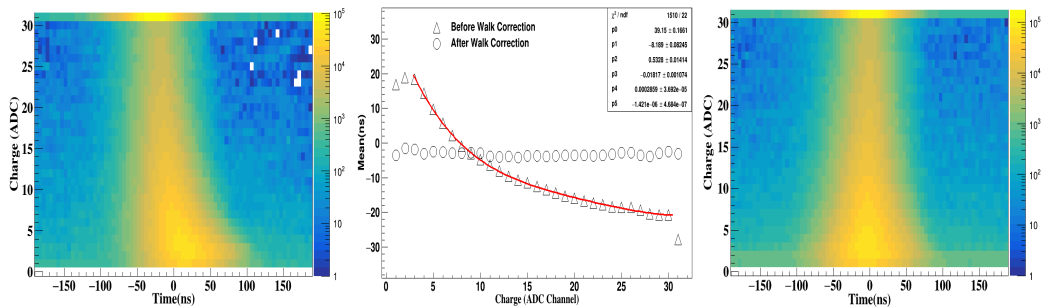


**Figure 6.** Left: Variation of the time difference between signals in GEM1 and one of the TOF modules (super module 0) with pulse height (in ADC unit) of GEM1. Middle: Variation of the mean (ns) of the time difference spectra with ADC before (upper triangle) and after (open circle) time-walk correction. The raw values are parameterized using a polynomial fit. Right: Variation of the time difference between GEM1 and one of TOF counter for different ADC values after time-walk correction.

163 The time correlation spectra are obtained for each FEB separately, and the extracted peak-  
 164 position after appropriate Gaussian fit provides the time-offset for all the channels of the corre-  
 165 sponding FEB. By implementing these FEB-to-FEB corrections on the entire data set, we have  
 166 made an effort to bring all the digis synchronization with those from T0 for further analysis. How-  
 167 ever, there could still be time-walk effects [16] on the signal timing due to varying signal strengths,  
 168 as can be seen from the 2D distribution of ADC vs. time difference for GEM1 in Fig. 6 (left). The  
 169 variation of the time difference peak position (ns) for the corresponding ADC bin is shown in Fig. 6  
 170 (middle). It has been fitted with a polynomial to find the parametric equation for the time-walk  
 171 correction. The 2D distribution after time-walk correction is shown in Fig. 6 (right). The mean  
 172 offset values for every FEB is now well peaked at around zero ns, by construction, as depicted in  
 173 Fig. 7 (left). Open circles denote the time-offset values for different FEBs (represented by ASIC  
 174 Id on the X-axis). For a few FEBs, these offsets were very high (in several  $\mu$ s) and exceeded the  
 175 scale of the plot. Eventually, all these offsets could be corrected (full circles). The width of the



176 time difference spectra provides the time resolution of the detector. Using a Gaussian fit, the sigma  
 177 ( $\sigma$ ) of this distribution for both before and after the time-walk correction has been shown in Fig. 7  
 178 (right). An improvement of 6-7 ns is observed after correction.

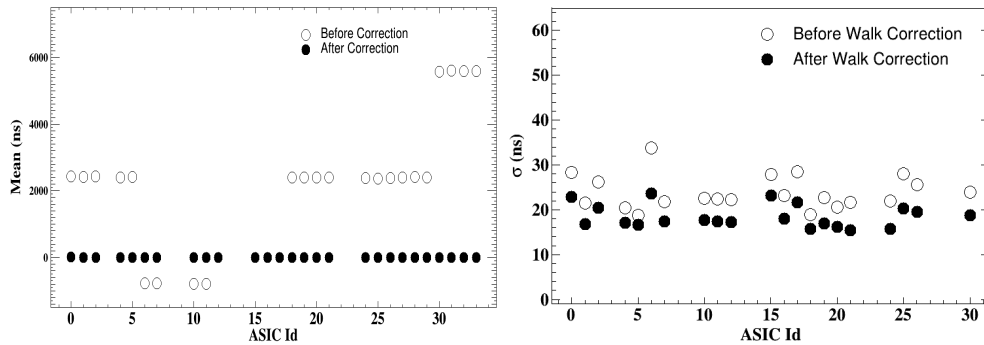


**Figure 7.** Left: Variation of the mean (ns) of time difference spectra for each ASIC with ASIC number before (open circle) and after (close circle) offset correction. Mean positions for a few ASICs are not shown here due to large offset value (several  $\mu$ s). Right: The variation of  $\sigma$  with ASIC number before (open circle) and after (close circle) time-walk correction. The ASIC Id for GEM1 is from 0 to 23, while those beyond belong to GEM2.

179 A deeper look at detector uniformity has been carried out at the level of pads/channels. The  
 180 2D-plot graphically display the variation in time resolutions (after time-walk correction) for about  
 181 1400 channels of GEM1 in Fig. 8 (left). This variation is observed to be of the order of 4-5 ns  
 182 from the mean value, which can be seen from the width of the 1-D distribution of  $\sigma$  (right panel of  
 183 Fig. 8).

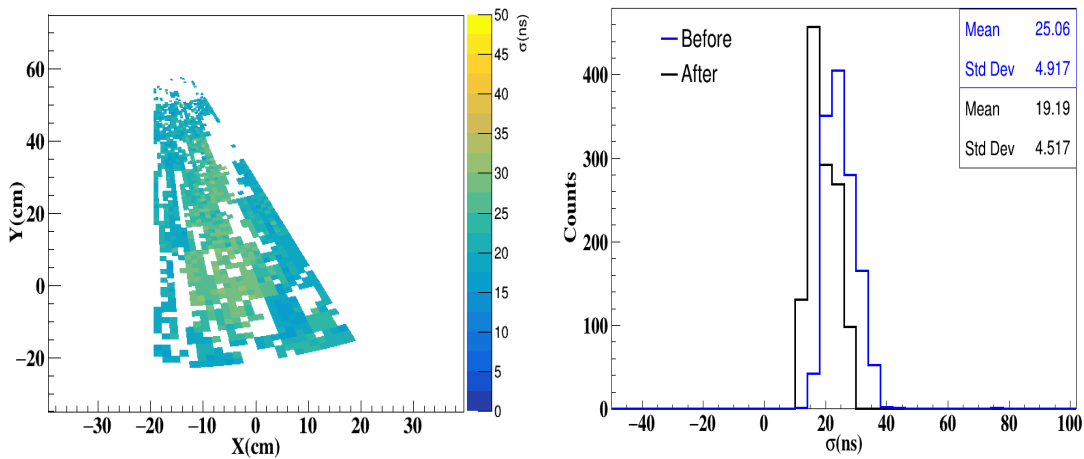


**Figure 8.** Left: Time resolution map on GEM1 plane. The z-axis is the  $\sigma$  (ns) of each pad. Right: 1-D distribution of time resolution for all the pads (shown left) before (Blue) and after (Black) time-walk correction.

184 In a self-triggered system, event building, as well as reconstruction, is a challenging task.  
 185 Using the timestamps of the signals from the detectors, an algorithm of building events by suitably  
 186 grouping digis in time was used. As a first attempt in this direction, we have used a time window  
 187 of 200 ns to group together the digis along with a condition of having at least one T0 and six TOF

188 digis within this time interval. This time window of 200 ns was considered based on the typical  
 189 time resolution of the detector subsystems as well as on rather moderate collision rates. All MuCh  
 190 digis inside this time window are clubbed together with the T0 and TOF digis forming events  
 191 subsequently.

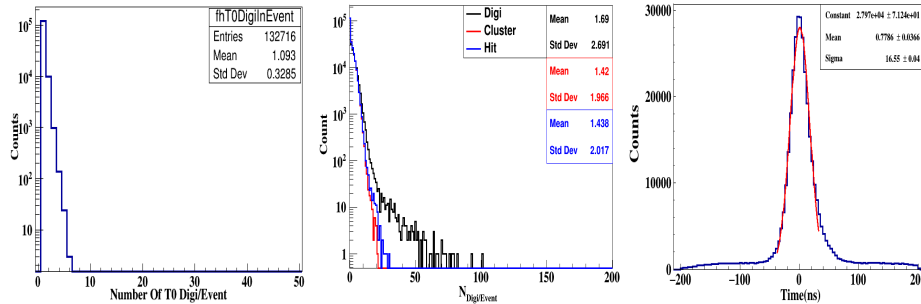


**Figure 9.** Left: Distribution of the number of T0 Digi / event. Middle: Distribution of number digi (black), Cluster (red) and Hits (blue) per event. Right: Time difference distribution between hits of GEM1 with T0 digi in the event.

192 As mentioned, the event building algorithm is still under investigation. One quality check for  
 193 the algorithm is to study the T0 distribution event by event. Ideally, for every collision, there should  
 194 be one T0 Digi. Each time window satisfying the hit-criteria is supposed to represent one collision,  
 195 implying that the number of T0 digis per event should typically average around “1”. This is revealed  
 196 in Fig. 9 (left), where the average number of T0 digis per event yields to be about 1.1 (matching  
 197 with our expectation within 10 %).

198 The event building was followed by cluster finding and hit reconstruction within the MuCh  
 199 modules. Each particle track that produces a signal in the detector may affect one or more pads  
 200 (digis). A nearest neighbor algorithm was used to club together with the digis in an event forming  
 201 a fired-pad clusters. Clusters having more than one local maximum were split further, thus forming  
 202 “Hits”. The middle panel of Fig. 9 shows systematically the event-by-event distributions of the  
 203 number of digis, the number of clusters, and finally, the number of “Hits” for GEM1. As a result of  
 204 the cluster splitting, the distribution of “Hits” is observed to be marginally wider than that for the  
 205 clusters. The time correlation of the MuCh “Hits” with T0 digis within an event is shown in Fig. 9  
 206 (right). During “Hit” reconstruction, the algorithm chooses the smallest time of the Digi within  
 207 the cluster; hence, the width of this time-correlation spectra is slightly smaller than that in Fig. 8  
 208 (right). The measured time resolution values at mCBM are pretty close to what has been measured  
 209 using single-particle beams [6]. The width of the time correlation spectra would play a crucial role  
 210 in optimizing the time window of the event building algorithm, particularly when operating at high  
 211 collision rates.

212 The X (cm) - Y (cm) distribution of hits for GEM1 (left) and GEM2 (right) are shown in  
 213 Fig. 10, revealing the detector acceptance. Figure 11 describes the cluster characteristics for the  
 214 hits in GEM1. The left panel shows the typical cluster size distribution for GEM1 at an operating  
 215 voltage of  $\Delta V_{GEM}(sum) \sim 1072$  V. The corresponding distribution of the cluster charge (fC) for the  
 216 entire GEM1 clusters is shown in the middle panel. Since we have used 5-bit ADC, a considerable  
 217 charge falls in the overflow bin (31 ADC channel), hence a spike at around 82 fC. Similar nature

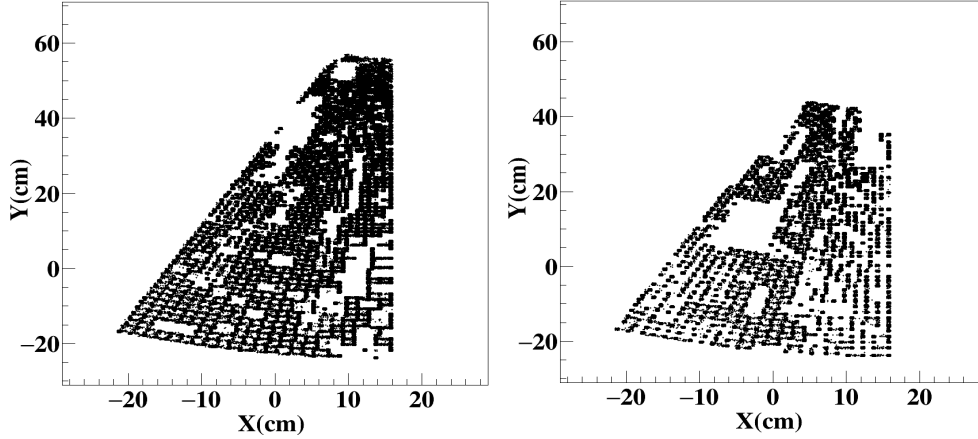


**Figure 10.** X (cm)-Y (cm) distribution of hits for GEM1 (left) and GEM2 (right) after hit reconstruction. The white spaces mostly correspond to the dead areas, mainly due to non-working FEBs and masked noisy pads/channels in the detector.

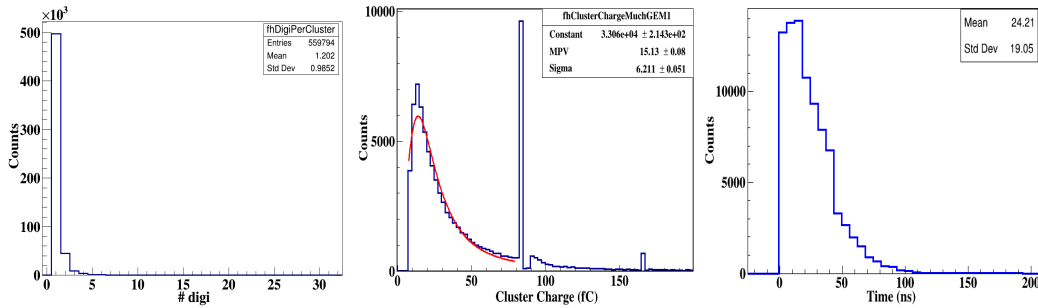


**Figure 11.** Left: Cluster size distribution for the entire GEM1 plane. Middle: Cluster charge (ADC) distribution for GEM1. The distribution is fitted with a Landau distribution. Right: Time separation of digis within clusters. The standard deviation yields to  $\sim 19$  ns.

218 of the cluster charge (fC) distribution has also been seen in response simulations (GEANT). The  
 219 cluster charge spectra are fitted with a Landau distribution, giving an MPV of 15.13 fC. Using the  
 220 MPV value, the gain at a summed GEM voltage of about 1072 V is estimated to be  $\sim 3.1 \times 10^3$ .  
 221 Within a reconstructed cluster, the distribution of time-difference of all the digis with respect to the  
 222 first Digi in time is shown in Fig. 11 (right). The RMS of this plot gives an idea about the time  
 223 spread between the digis of a MuCh cluster. It is observed that for more than 90% of times, the  
 224 separation between the Digis is within 50 ns. This information is useful for optimizing the time  
 225 separation between clusters related to the CBM 4D tracking.

226 The relative gain of the detector was measured at various positions on the detector plane, as  
 227 shown in Fig. 12 (left). Each position number represents a specific zone in the detector, which is  
 228 displayed in the right panel of the same figure. The gain distribution is observed to be uniform  
 229 at the level of about 15%. The readout plane has pads of varying granularity. The cluster size  
 230 distribution in different regions of the detector have been measured. The variation of the average  
 231 cluster size for different granularity zones is shown in Fig. 13. Statistical errors are included but  
 232 within the marker size. Further contributions due to dead areas, noise, thresholds, fluctuations in  
 233 gain, etc., are not considered. The different regions are indicated by numerals, and the adjoining

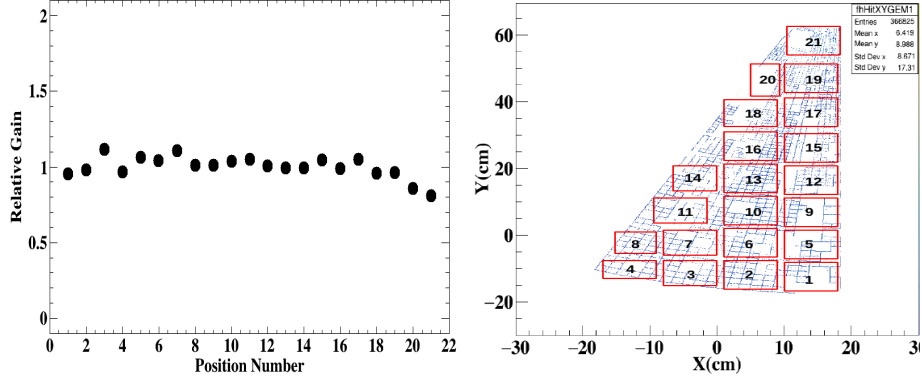


**Figure 12.** Left: Relative gain of the detector in different regions for GEM1. Right: Position numbers used in the left plot is indicated on the detector plane.

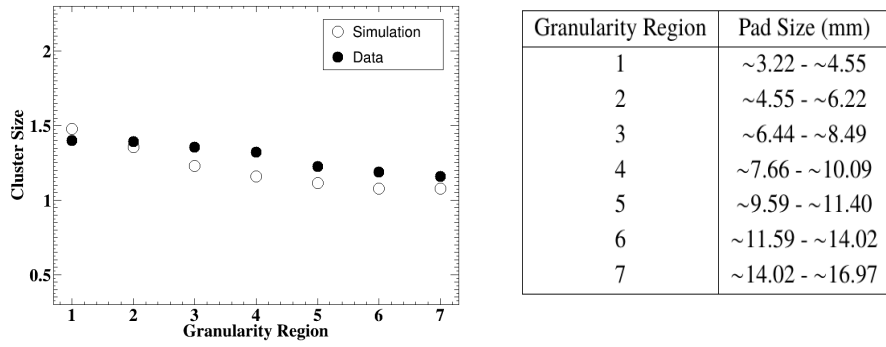


**Figure 13.** Left: Variation of cluster size at different granularity regions. Right: Table for granularity regions and their respective pad sizes.

234 table in the right indicate the corresponding granularity. The corresponding values obtained from  
 235 GEANT simulations in the mCBM environment and realistic GEM module configurations are also  
 236 overlaid, and the two values are found to match closely within 10%.

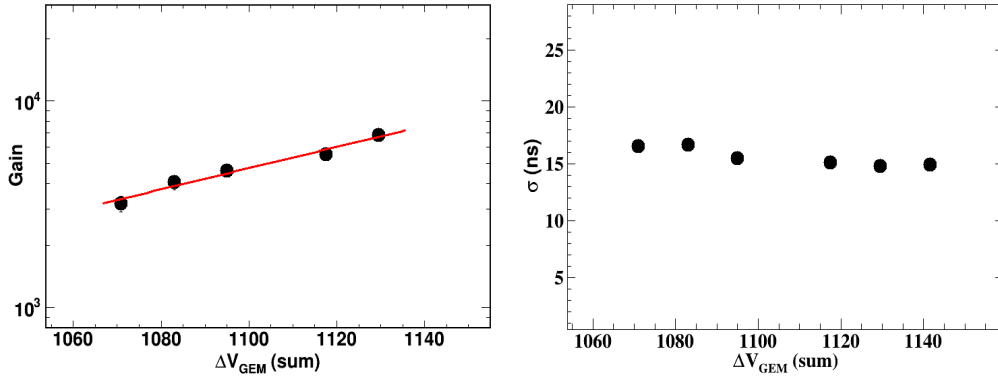


**Figure 14.** The variation of gain (left) and time resolution (right) of the detector with the GEM voltages.

237 Detector characteristics have been studied as a function of applied GEM voltages. The first  
 238 among these is the variation of detector gain with the GEM voltage. As shown in Fig. 14 (left),  
 239 the gain increases exponentially with increasing voltage, as expected. The right panel shows the  
 240 variation of time resolution with applied voltage. The time resolution is observed to saturate at

241 around 15 ns. The errors (statistical) on the data points in both the panels are within the marker  
 242 size. The variation of the cluster size with voltage is shown in Fig. 15 (left). The slight increase,  
 243 which is also observed in simulation, is due to increased gain at higher voltages. The variation of  
 244 average hits per event is shown in Fig. 15 (right). The curve shows a rising trend, indicative of the  
 245 effect due to increased efficiency at higher GEM voltages.

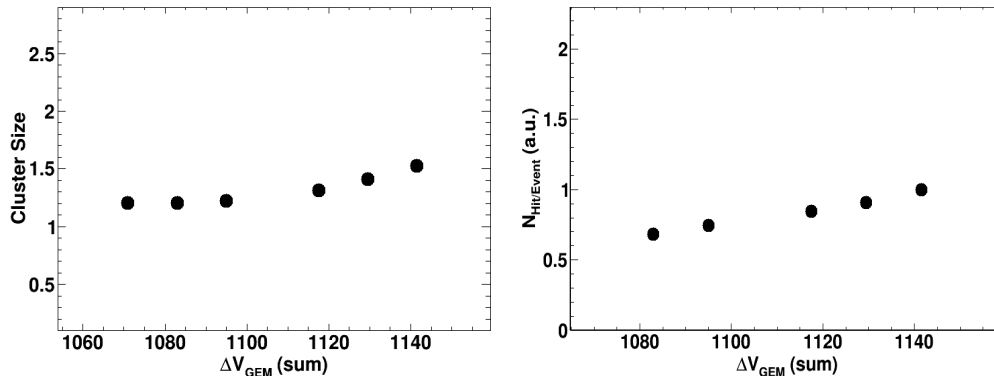


**Figure 15.** Variation of cluster size with voltage (left). Variation of average Hit/event with GEM voltage.

246 Using the hits registered on the different detector planes within the built events described in the  
 247 above section, we try to investigate the spatial correlation. Figure 16 displays the spatial correlation  
 248 in X and Y between GEM1 and GEM2. The range of the correlation line observed in both X and  
 249 Y matches with the observations of the 2D-Hits plot of Fig. 10. The region of common overlap in  
 250 X and Y is highlighted in the elliptical ring. It must be stated that the event building is required to  
 251 make the correlation lines cleanly visible, which is not feasible while scanning complete time-slices  
 252 of 10 ms overlaying many events.

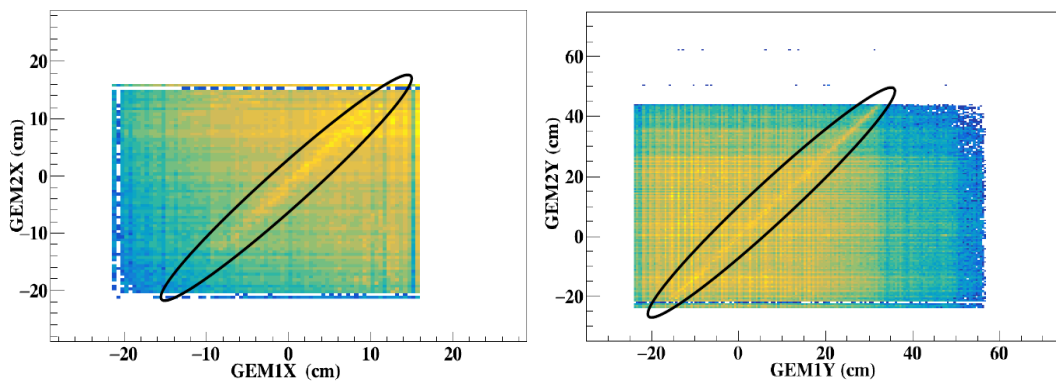


**Figure 16.** Spatial correlation in X (cm) and Y (cm) between GEM1 and GEM2 hits

253 Further studies related to extracting detector efficiencies, multiplicity distributions, and the  
 254 performance at high collision rates are expected to be carried out in the upcoming mCBM campaigns.

## 255 5 Summary

256 We have commissioned large-size trapezoidal GEM modules designed for the CBM-MuCh system  
 257 in the ongoing mCBM experiment at GSI. The modules have been tested under realistic experimental

258 conditions in nucleus-nucleus collisions. Data have been taken in November and December 2019  
259 for Ar + Au collisions at 1.7 AGeV beam kinetic energy. A preliminary CBM data analysis chain  
260 based on the CbmRoot software framework has been applied to the data. First results have been  
261 obtained by studying the detector performance in terms of on-spill and off-spill count rates, time  
262 correlations and resolution.

263 Noisy channels were identified using the off-spill part of the data. Appropriate offset corrections  
264 have been implemented to enable a first event building by applying a time-cluster search. For the  
265 first time, a cluster and hit reconstruction has been performed on the MuCh detector data taken  
266 with the free-streaming CBM DAQ system. The cluster-size and cluster-charge characteristics in  
267 different zones of the detector have been studied as well. The gain of the detector has been calculated  
268 using the cluster-charge of reconstructed hits and its variation with the GEM voltage. An average  
269 time resolution of about 15 ns was measured for the tested GEM module. The uniformity of the  
270 detector response has been studied in terms of the relative gain-plot using the mean of the cluster  
271 charge distribution zone-wise and in terms of the time resolution measured for a large number of  
272 pads throughout the detector area. An RMS of 4-5 ns describes the spread in the time resolutions  
273 measured over the entire area of the detector. The average dispersion of the digis in time within  
274 a cluster has been studied as well. Performing a first event building on digi-level, clear spatial  
275 correlations between both GEM modules (GEM1 and GEM2) were observed.

## 276 Acknowledgments

277 AK acknowledges the receipt of a DAE-HBNI Fellowship. The work has been funded by DAE,  
278 India. The results presented here are based on the experiment S471 (mCBM), which was performed  
279 at the beam line/infrastructure HTD at the GSI Helmholtzzentrum fuer Schwerionenforschung,  
280 Darmstadt (Germany) in the frame of FAIR Phase-0. We acknowledge the GSI team for the  
281 intensive help and fruitful discussions.

## 282 References

- 283 [1] The CBM experiment. <https://www.cbm.gsi.de/>.
- 284 [2] The Facility for Antiproton and Ion Rsearch FAIR. <https://fair-center.eu/>.
- 285 [3] Subhasis Chattopadhyay, Yogendra Pathak Viyogi, Peter Senger, Walter F. J. Müller, and Christian J.  
286 Schmidt, editors. *Technical Design Report for the CBM : Muon Chambers (MuCh)*. GSI, 2015.  
287 <https://repository.gsi.de/record/161297>.
- 288 [4] A.K. Dubey et al. GEM detector development for CBM experiment at FAIR. *Nucl. Instrum. Meth. A*,  
289 718:418 – 420, 2013. <https://doi.org/10.1016/j.nima.2012.10.043>.
- 290 [5] A.K. Dubey et al. Testing of triple-GEM chambers for CBM experiment at FAIR using self-triggered  
291 readout electronics. *Nucl. Instrum. Meth. A*, 755:62 – 68, 2014.  
292 <https://doi.org/10.1016/j.nima.2014.04.027>.
- 293 [6] Rama Prasad Adak et al. Performance of a large size triple GEM detector at high particle rate for the  
294 CBM Experiment at FAIR. *Nucl. Instrum. Meth. A*, 846:29 – 35, 2017.  
295 <https://doi.org/10.1016/j.nima.2016.12.004>.

- 296 [7] The Phase-2 Upgrade of the CMS Muon Detectors. Technical Report CERN-LHCC-2017-012.  
297 CMS-TDR-016, CERN, Geneva, Sep 2017. <https://cds.cern.ch/record/2283189>.
- 298 [8] Upgrade of the ALICE Time Projection Chamber. Technical Report CERN-LHCC-2013-020.  
299 ALICE-TDR-016, CERN, Oct 2013. <https://cds.cern.ch/record/1622286>.
- 300 [9] Alessandro Cardini, Giovanni Bencivenni, and Patrizia De Simone. The Operational Experience of  
301 the Triple-GEM Detectors of the LHCb Muon System: Summary of 2 Years of Data Taking.  
302 Technical Report LHCb-PROC-2012-060. CERN-LHCb-PROC-2012-060, CERN, Geneva, Nov  
303 2012. <https://cds.cern.ch/record/1495070>.
- 304 [10] H Klest. Overview and design of the sPHENIX TPC. *Journal of Physics: Conference Series*,  
305 1498:012025, apr 2020. <https://doi.org/10.1088/1742-6596/1498/1/012025>.
- 306 [11] W. Anderson et al. Design, construction, operation and performance of a Hadron Blind Detector for  
307 the PHENIX experiment. *Nucl. Instrum. Meth. A*, 646(1):35 – 58, 2011.  
308 <https://doi.org/10.1016/j.nima.2011.04.015>.
- 309 [12] Ablyazimov T et al. Challenges in QCD matter physics -- The scientific programme of the  
310 Compressed Baryonic Matter experiment at FAIR. *Eur. Phys. J. A*, 53(3):60, 2017.  
311 <https://doi.org/10.1140/epja/i2017-12248-y>.
- 312 [13] The mCBM experiment. to be published, see experiment  
313 proposal: <http://dx.doi.org/10.15120/GSI-2019-00977>.
- 314 [14] Ajit Kumar et al. Testing of large size GEM detector with Pb + Pb collision at CERN-SPS. *DAE*  
315 *Symp. Nucl. Phys.*, 62:1006–1007, 2017. <https://cds.cern.ch/record/2674709>.
- 316 [15] mCBM@SIS18, A CBM full system test-setup for high-rate nucleus-nucleus collisions at GSI / FAIR,  
317 The CBM Collaboration. Technical report, 2017. <http://dx.doi.org/10.15120/GSI-2019-00977>.
- 318 [16] K. Kasinski et al. Characterization of the STS/MUCH-XYTER2, a 128-channel time and amplitude  
319 measurement IC for gas and silicon microstrip sensors. *Nucl. Instrum. Meth. A*, 908:225 – 235, 2018.  
320 <https://doi.org/10.1016/j.nima.2018.08.076>.
- 321 [17] Rafal Kleczek. Analog front-end design of the STS/MUCH-XYTER2—full size prototype asic for  
322 the CBM experiment. *Journal of Instrumentation*, 12(01):C01053–C01053, 2017.  
323 <https://doi.org/10.1088/1748-0221/12/01/c01053>.
- 324 [18] A. Kumar et al. Testing of triple GEM prototypes for the CBM Muon Chamber system in the mCBM  
325 experiment at the SIS18 facility of GSI. *Journal of Instrumentation*, 15(10):C10020–C10020, oct  
326 2020. <https://doi.org/10.1088/1748-0221/15/10/c10020>.
- 327 [19] Laura Franconi Andrey Marinov. Status of no-stretch no-spacer GEM assembly, the NS2 technique  
328 method and experiment result. 2012. <https://indico.cern.ch/event/176664/contributions/1442160/>.
- 329 [20] Ajit Kumar et al. Operating large size GEM detectors using a novel optocoupler based biasing scheme  
330 for the Muon Chamber system of CBM experiment. *Nucl. Instrum. Meth. A*, 958:162905, 2020.  
331 <https://doi.org/10.1016/j.nima.2019.162905>.
- 332 [21] D. Nag et al. Study and design of a water based cooling system for MuCh CBM. *CBM Progress*  
333 *Report*, pages 90–91, 2016. <https://repository.gsi.de/record/201318>.
- 334 [22] The CbmRoot Framework. <http://computing.gitpages.cbm.gsi.de/cbmroot/>.